Lithiated Nanocrystals

DOI: 10.1002/anie.201408108

Colloidal Nanocrystals of Lithiated Group 14 Elements**

*Jacqueline E. Cloud, Yonglong Wang, Tara S. Yoder, Lauren W. Taylor, and Yongan Yang**

Abstract: *The synthesis of colloidal nanocrystals (NCs) of lithiated group 14 elements (Z = Si, Ge, and Sn) is reported, which are $Li_{4.4}Si$, $Li_{3.75}Si$, $Li_{4.4}Ge$, and $Li_{4.4}Sn$. Li_xZ compounds are highly reactive and cannot be synthesized by existing methods. The success relied on separating the surface protection from the crystal formation and using a unique passivating ligand. Bare Li_xZ crystals were first produced by milling elemental Li and Z in an argon-filled jar. Then, under the assistance of additional milling, hexyllithium was added to passivate the freshly generated Li_xZ NCs. This ball-milling-assisted surface protection method may be generalized to similar systems, such as Na_xZ and K_xZ. Moreover, $Li_{4.4}Si$ and $Li_{4.4}Ge$ NCs were conformally encapsulated in carbon fibers, providing great opportunities for studying the potential of using Li_xZ to mitigate the volume-fluctuation-induced poor cyclability problem confronted by Z anodes in lithium-ion batteries.*

Lithium-ion batteries (LIBs) are widely considered to be crucial energy conversion and storage devices in the global pursuit of decreasing the dependence on fossil fuels and increasing clean energy technologies (such as electric vehicles), in order to build an energy-sustainable future.[1–3] To realize this potential, one of the requirements is to replace the conventional graphite anode.[4,5] Among all candidates, three group 14 elements (Z = Si, Ge, and Sn) have been regarded as the most promising ones.[4–15] Their theoretical gravimetric charge capacities are 4200, 1625, and 994 $mAhg^{-1}$, respectively, up to ten times higher than that of graphite (372 $mAhg^{-1}$).[4–10,11,16–18] Si is attractive for large-scale applications, because of its earth abundance, cost-effectiveness, and well-established commercial history;[4,5,7,8,19–23] Ge and Sn are appealing for high-power LIBs, because of their higher electrical conductivities and Li-ion diffusivity.[16,24,25] Different from graphite, Z anodes store Li ions through the alloying-based conversion mechanism, in which their crystal structures change dramatically with the lithiation/delithiation cycles.[8,26–28] Consequently, the repeated volume fluctuations (up to 400%) damage the electrode quickly and result in poor cyclability.[4–10,29–31] To date, fundamental studies on Z electrodes have provided a good understanding of the failure mechanism and many mitigation strategies have been explored.[20–23,29–41] However, practical Z anodes are presently unrealistic; a deeper fundamental understanding and new mitigation strategies are required.

One promising approach is to study lithiated Z electrodes (Li_xZ). The reasons are as follows. First, in a practical LIB, Li_xZ is equally important as Z for a Z anode, which can start with either the non-lithiated or the prelithiated states. Second, evidence is emerging that the premade Li_xZ is different from the in situ electrochemically made Li_xZ.[42,43] While Li_xZ has five thermodynamic states ($x = 4.4$, 3.25, 2.33, 1.71, and 1.0) and one metastable state ($Li_{3.75}Si$), only $Li_{4.4}Z$ and $Li_{3.75}Z$ have been observed in electrochemical cells.[42,44] The electrical and ionic conductivities of Li_xZ are several orders of magnitude higher than those of Z.[43,45] Delithiation of Li_xZ produces amorphous Z, a form showing superior cyclability compared to crystalline Z.[8,46,47] Thus, the study of premade Li_xZ will deepen and broaden our fundamental understanding of Z anodes. Third, Li_xZ may provide an unusual approach to effectively accommodate the volume fluctuation. To date, the most elegant and effective strategy is to preset void space contiguous to Z nanoparticles, referred to as void space manipulation.[20,48] The main advantage of starting with Li_xZ is the possibility of providing adequate void space for every Li_xZ particle regardless of particle size and shape, since the necessary void space is created through electrochemical delithiation. This strategy can be denoted as reverse void space manipulation. In addition, toward large-scale applications of LIBs, the remarkable advancements in developing high-performance sulfur cathodes require prelithiated anodes,[49] for which Si is the most attractive, as Si and S offer the highest charge capacity among all solid anode and cathode materials, respectively.[50–52] Therefore, it is of scientific and technological importance to systematically study Li_xZ.

For such a study, colloidal Li_xZ nanocrystals (NCs) are desirable, considering three factors. First, NCs may enable high charging/discharging rates, because of their large surface areas and small diffusion dimensions for Li ions.[28,29,33] Second, colloidal NCs are preferred structures for an effective fabrication of Li_xZ@carbon core–shell composites,[53,54] in order to practice the strategy of reverse void space manipulation. Third, colloidal NCs are suitable for individual particle characterization with in situ imaging techniques, preferred for mechanistic studies.[8,16,27,46,55]

However, the synthesis of colloidal Li_xZ NCs remains a challenging task. Li_xZ compounds are alloyed Li and Z,

[*] J. E. Cloud, Dr. Y. Wang, T. S. Yoder, L. W. Taylor, Prof. Y. Yang
Department of Chemistry and Geochemistry
Colorado School of Mines, 1012 14th Street, Golden, CO 80401 (USA)
E-mail: yonyang@mines.edu
Homepage: http://inside.mines.edu/~yonyang/Home.html

[**] This work is financially supported by the Startup Fund for Y.Y. from the Colorado School of Mines (CSM), the proof-of-concept grant (grant number 11833) from the Colorado Office of Economic Development and International Trade (COEDIT) and the Office of Technology Transfer of CSM, and National Science Foundation through the Renewable Energy Materials Research Science and Engineering Center (REMRSEC) under grant number DMR-0820518.

Supporting information for this article is available on the WWW under http://dx.doi.org/10.1002/anie.201408108.

 © 2014 Wiley-VCH Verlag GmbH & Co. KGaA, Weinheim

featured with the chemical properties of individual elements.[43] They, like Li, are highly reactive and incompatible with all conventional ligands, such as carboxylic acids, thiols, amines, and polyols.[56] Therefore, an unconventional strategy is imperative for synthesizing colloidal Li_xZ NCs. To date, only three methods have been reported to synthesize Li_xZ: melt quenching,[57–62] electrochemical lithiation,[42,44] and mechanical ball milling.[43,63–66] For melt quenching, the method used to establish Li–Z phase diagrams,[57–61] a post-synthesis treatment will be necessary to convert the as-synthesized bulk materials into NCs. Electrochemical lithiation inevitably introduces surface contamination, making ligand attachment impossible.[42,44] In contrast, mechanical ball milling directly produces NCs; the remaining challenge is how to attach an appropriate ligand to accomplish the surface protection.[43,63–66]

Herein we report the synthesis of colloidal Li_xZ ($Li_{4.4}Si$, $Li_{3.75}Si$, $Li_{4.4}Ge$, and $Li_{4.4}Sn$) NCs using a two-step protocol: 1) synthesis of bare Li_xZ NCs by ball-milling elemental Li and Z; and 2) surface protection by attaching the ligand hexyllithium (HL) under the assistance of additional milling. Moreover, $Li_{4.4}Si$ and $Li_{4.4}Ge$ NCs are encapsulated in carbon fibers, creating the opportunity of studying the effectiveness of reverse void space manipulation.

Figure 1 shows the synthesis of colloidal Li_xZ NCs, using $Li_{4.4}Si$ as the model system. The key step of ball-milling-assisted surface protection is illustrated in Figure 1 a. $Li_{4.4}Si$ powder was premade by milling Li grains and Si powder in an argon-filled milling jar mounted on a high-energy ball mill.

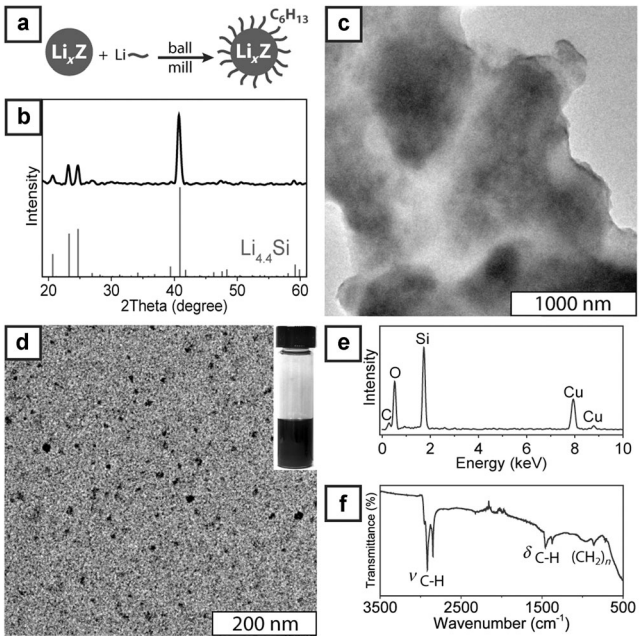

Figure 1. Synthesis of colloidal Li_xZ NCs using $Li_{4.4}Si$ as the model system. a) Cartoon depicting the ball-milling-assisted surface protection using HL (Li-C_6H_{13}) as the ligand. b) XRD profile of the synthesized colloidal $Li_{4.4}Si$ NCs (black) compared to the standard (JCPDS: 04-007-0820). c) TEM image of agglomerated $Li_{4.4}Si$ NCs. d) TEM image of colloidal $Li_{4.4}Si$ NCs, where the inset shows an optical image of the obtained colloidal solution. e) EDX spectrum of colloidal $Li_{4.4}Si$ NCs. f) FTIR spectrum of colloidal $Li_{4.4}Si$ NCs.

The protocol modified a literature method,[64] using hexane instead of the typically used dodecane as the lubricant in order to ease the post-synthesis purification, benefiting from the decreased viscosity and boiling-point of the lubricant. Then, the ligand HL was added and the mixture was ball milled again (Figure 1 a). Consequently, ball milling constantly separated the previously made and aggregated NCs; the presence of HL led to an instant and effective surface protection of the freshly exposed NC surfaces. The obtained crystalline product was characterized by X-ray diffraction (XRD) to be phase-pure $Li_{4.4}Si$ (Figure 1 b), while an amorphous phase could not be excluded because of its insensitivity to XRD. Both ball milling and HL-addition were critical; otherwise, only micrometer-sized aggregates would be obtained, as shown in the transmission electron microscopy (TEM) image (Figure 1 c). The obtained colloidal $Li_{4.4}Si$ NCs were highly dispersed (8.3 ± 2.3 nm in diameter) and soluble in hexane, as shown by a TEM image and an optical image in Figure 1 d. The corresponding energy-dispersive X-ray (EDX) spectrum (Figure 1 e) showed the expected results: a strong Si signal originating from the sample, in which Li was not detectable by EDX; a C signal from the carbon support on the Cu grid and the HL carbon chain; and an O signal from the surface oxidation of $Li_{4.4}Si$ and Cu grid. Furthermore, the Fourier transform infrared (FTIR) spectrum (Figure 1 f) confirmed the presence of HL on the surface of the obtained colloidal $Li_{4.4}Si$ NCs, since the presence of free HL and residual hexane could be excluded on the bases of their low boiling points and sufficient purification treatment. The peaks at 2848 and 2916 cm^{-1} were indexed to the C–H stretching mode (ν_{C-H}); the peaks at 1462 and 1376 cm^{-1} were assigned to the C–H bending mode (δ_{C-H}); and the peak at 719 cm^{-1} was from the $(CH_2)_n$ rocking mode.[67]

As aforementioned, the high reactivity of Li_xZ made it impossible to use any conventional ligand.[56] Thus, our ligand selection had to focus on compounds containing only C, H, and Si or Li, to avoid causing detrimental reactions to Li_xZ and introducing impurities to the system. The use of triethylsilane (TES, Et_3SiH) during the synthesis of $Li_{4.4}Si$ produced an unknown compound with a significant amount of unreacted Si and no Li_xSi, as shown by the XRD data in Figure 2 a. TES failed to serve as a ligand and somehow prevented the formation of Li_xSi. In contrast, the use of HL turned out to be an exciting success, because of two key features. First, HL can function as a ligand to passivate the particle surface through Z-LiC_6H_3 bonds, without breaking the built-in Li–C bonds. Second, the stabilizing solvent for the HL reagent, hexane, is the preferred lubricant for producing Li_xZ and causes no harm to the synthesis.

With the success of methodology exploration, we tried to control the sizes of $Li_{4.4}Si$ NCs. Three variables were investigated: 1) the moment of the ligand addition, 2) the size of the milling balls, and 3) the milling duration. When HL was added at the beginning of mixing Li and Si, the obtained product was a mixture of $Li_{3.75}Si$ and $Li_{4.4}Si$, as shown by the XRD data in Figure 2 b. The existence of $Li_{3.75}Si$ was due to the decreased availability and reactivity of Li resulting from clustered Li that was strongly passivated by HL.[68] In the literature, it has been found that the size of the milling balls

 © 2014 Wiley-VCH Verlag GmbH & Co. KGaA, Weinheim

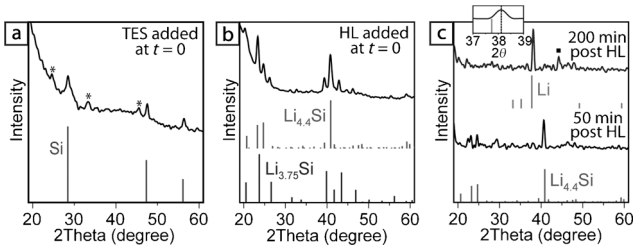

Figure 2. XRD data of the products in the course of synthesizing colloidal $Li_{4.4}Si$ NCs. a) TES was added in the first step. b) HL was added in the first step. c) The milling duration in the second step was shortened to 50 minutes and prolonged to 200 minutes, respectively. The standard patterns are for Si (JCPDS: 04-001-7247), $Li_{4.4}Si$ (JCPDS: 04-007-0820), $Li_{3.75}Si$ (JCPDS: 04-007-0820), and Li (JCPDS: 04-007-4180). The symbols (*) and (■) are assigned to an unknown product and a Fe (JCPDS: 04-003-7116) contaminant from the milling jar, respectively.

can affect particle size and size distribution of the produced NCs.[69,70] However, when we decreased the ball size from 12.7 to 6.35 mm during the second step of the synthesis, the particle size remained similar (7.1 ± 2.6 nm, Figure S1a). This was likely due to the dwarfed effect of the ball size in a high-energy ball mill. When the milling duration in the second step was decreased from the typical value of 100 to 50 minutes, no well-dispersed NCs could be observed by TEM (Figure S1b), while the product was still $Li_{4.4}Si$ as shown by the XRD data in Figure 2c. After prolonging the duration to 200 minutes, the product could only be index to Li (Figure 2c). Since the starting material in the second step was premade $Li_{4.4}Si$, it was surprising to observe its disappearance and the appearance of Li without signals of crystalline Si. Our speculation was that extended milling broke $Li_{4.4}Si$ into Li and amorphous Si because of the presence of HL;[68] the upward shift of the diffraction peak by 0.37° (the inset in Figure 2c) versus the standard peak at 38.11° (JCPDS: 04-007-4180) was ascribed to decreased lattice constants due to the stress caused by high-energy ball milling.[42] In the future the challenge of size-control will be tackled again upon access to a planetary ball mill, which is gentler than the currently used high-energy ball mill.

The method described above for synthesizing highly dispersed colloidal $Li_{4.4}Si$ NCs was then applied to synthesize colloidal $Li_{3.75}Si$, $Li_{4.4}Ge$, and $Li_{4.4}Sn$ NCs, as shown in Figure 3. For $Li_{3.75}Si$, all XRD peaks (Figure 3a) shifted to smaller angles versus those in the standard (stick patterns, JCPDS: 04-007-0820), despite consistent diffraction patterns and relative intensities. A comprehensive literature survey revealed that $Li_{3.75}Si$ crystals synthesized using different methods, that is, electrochemical lithiation of crystalline Si ($Li_{3.75}Si$-c),[71] electrochemical lithiation of amorphous Si ($Li_{3.75}Si$-a),[17,72] planetary ball milling of Li and crystalline Si ($Li_{3.75}Si$-pb),[43] and high-energy ball milling of Li and crystalline Si ($Li_{3.75}Si$-hb),[73] presented systematic shifts in all XRD peaks. Recently, Zeng et al. reported that all XRD peaks of $Li_{3.75}Si$-c continuously shifted to larger angles with increasing externally applied pressure.[42] According to their results,[42] we inferred that $Li_{3.75}Si$ made by different methods possess different lattice-constants (internal-pressures), increasing (decreasing) in the order of $Li_{3.75}Si$-c, $Li_{3.75}Si$-a $\approx$ $Li_{3.75}Si$-hb, and $Li_{3.75}Si$-pb. The corresponding EDX spectrum of colloidal $Li_{3.75}Si$ NCs (Figure 3b) showed the expected results, as discussed for Figure 1e. The TEM measurement (Figure 3c) showed that the obtained $Li_{3.75}Si$ NCs were spherical particles with an average diameter of 7.1 ± 2.5 nm. The success of synthesizing colloidal $Li_{3.75}Si$ NCs was a result of decreasing the molar ratio of HL:$Li_{3.75}Si$ to 4.8:1 from the typical value of 8.8:1, at which the product was a mixture of Li, $Li_{3.75}Si$, and amorphous Si (Figure S2). The reason Li and amorphous Si was produced was very likely the same as in Figure 2c.

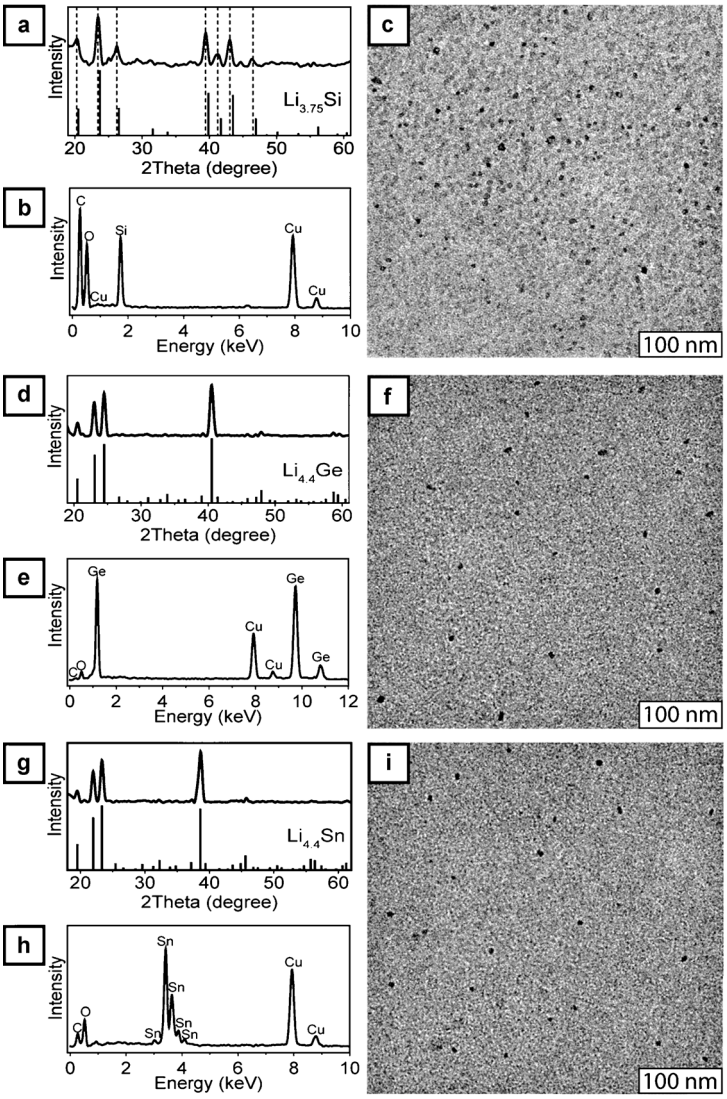

Figure 3. Characterization of colloidal $Li_{3.75}Si$ NCs (a–c), $Li_{4.4}Ge$ NCs (d–f), and $Li_{4.4}Sn$ NCs (g–i), using XRD (a, d, and g), EDX (b, e, and h), and TEM (c, f, and i). The XRD standards are for $Li_{3.75}Si$ (JCPDS: 04-007-0820), $Li_{4.4}Ge$ (JCPDS: 04-003-6445), and $Li_{4.4}Sn$ (JCPDS: 04-003-6446).

 © 2014 Wiley-VCH Verlag GmbH & Co. KGaA, Weinheim

Following the same protocol, colloidal $Li_{4.4}Ge$ NCs (Figure 3d–f) and $Li_{4.4}Sn$ NCs (Figure 3g-i) were also synthesized, as confirmed by XRD, EDX, and TEM. Both materials were well-dispersed nanospheres with average diameters of 5.3 ± 1.4 nm for $Li_{4.4}Ge$ and 5.3 ± 1.1 nm for $Li_{4.4}Sn$, respectively. The synthesis of $Li_{4.4}Sn$ in the first step required 300 minutes of ball milling, three times as long as the 100 minutes needed for $Li_{4.4}Si$ and $Li_{4.4}Ge$. If only 100 minutes of ball milling was applied, the product was a mixture of elemental Sn and $Li_{4.4}Sn$ (Figure S3). The need for extra milling time to synthesize $Li_{4.4}Sn$ was ascribed to the malleability and larger diameter (1.0 mm) of the Sn wires used, different from the brittle Si powder (325 mesh) and Ge grains.

Toward the goal of studying electrochemical properties of individual particles, we tried to encapsulate the synthesized colloidal $Li_{4.4}Si$ and $Li_{4.4}Ge$ NCs in electrospun carbon fibers (CFs), using the technique we previously used to load colloidal Ag NCs in CFs.[74] The first step was to fabricate Li_xZ NC-loaded polyacrylonitrile (PAN) fibers, using the electrospinning setup depicted in Figure 4a. Then, the

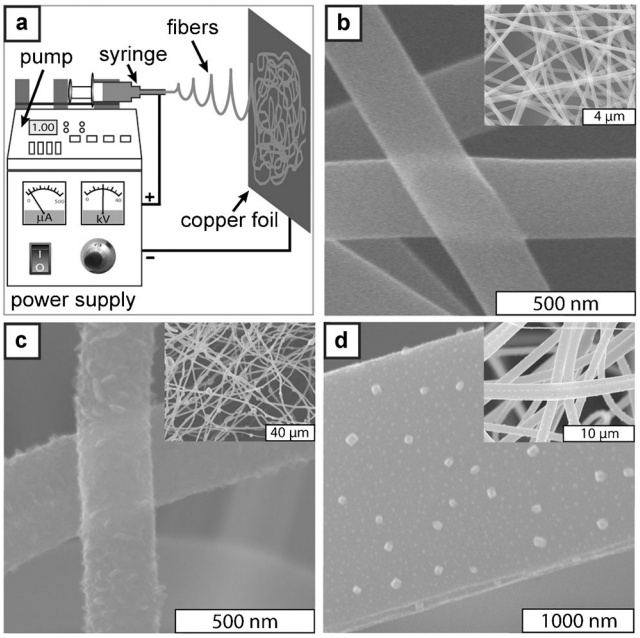

Figure 4. Synthesis and characterization of $Li_{4.4}Si$- and $Li_{4.4}Ge$-loaded CFs. a) Cartoon depicting the electrospinning setup, where a syringe is loaded with an *N*,*N*-dimethylformamide (DMF) solution containing PAN and Li_xZ NCs, a syringe pump is used to control the flow rate of the solution, a copper foil is the fiber collector, and a power supply is employed to apply a high voltage between the syringe and the copper foil. b–d) SEM images with lower magnification insets for b) bare CFs, c) $Li_{4.4}Si$@CFs, and d) $Li_{4.4}Ge$@CFs.

Li_xZ@PAN fibers were heated at 600 °C for one hour to pyrolyze PAN into carbon, producing Li_xZ@CFs. After the carbonization treatment, the HL ligands on the NC surfaces were expected to pyrolyze without introducing any impurities into the system, which is highly desirable. PAN was selected because its derived carbon is widely used to encapsulate electrode materials for LIBs.[75–77] Bare CFs, as shown by the SEM images in Figure 4b, are featured with smooth surfaces and straight edges. In contrast, the SEM images in Figure 4c present particulate features throughout the CFs, indicating the encapsulation of $Li_{4.4}Si$ NCs, which is further corroborated by the Si signal in the corresponding EDX spectrum (Figure S4a). In the Raman spectra of $Li_{4.4}Si$@CFs and CFs (Figure S5), the similar D and G bands indicate the comparable carbon quality.[75,78] The SEM images of $Li_{4.4}Ge$@CFs shown in Figure 4d present clearer features of encapsulated $Li_{4.4}Ge$ NCs. Considering the actual sizes (5.3 ± 1.4 nm) of colloidal $Li_{4.4}Ge$ NCs, we assigned the smaller spherical features (33 ± 5 nm) to slightly aggregated NCs and the larger spherical features (80 ± 8 nm) to heavily aggregated NCs. The presence of $Li_{4.4}Ge$ NCs in CFs was also supported by a strong Ge signal in the corresponding EDX spectrum (Figure S4b). The success of fabricating Li_xZ@CFs will allow us to investigate the reverse void space manipulation concept in the future.

In conclusion, we have reported an unconventional method for synthesizing four types of spherical, colloidal NCs of lithiated group 14 elements (Z = Si, Ge, and Sn), specifically, $Li_{4.4}Si$ (8.3 ± 2.3 nm), $Li_{3.75}Si$ (7.1 ± 2.5), $Li_{4.4}Ge$ (5.3 ± 1.4 nm), and $Li_{4.4}Sn$ (5.3 ± 1.1 nm). The success results from overcoming the incompatibility of the Li_xZ compounds with all conventional passivating ligands. The first critical factor is to separate the surface protection from the crystal formation, that is, bare Li_xZ crystals are first produced by milling elemental Li and Z in an argon-filled jar. The second factor is the use of a unique passivating ligand, that is, hexyllithium was mixed with the previously made bare Li_xZ crystals under the assistance of additional milling to passivate the freshly generated Li_xZ NCs. To the best of our knowledge, hexyllithium as a passivating ligand has not been demonstrated in the literature; colloidal NCs of binary compounds of high reactivity as Li_xZ have not been reported either. This ball-milling-assisted surface protection method may also be applicable for making similar colloidal NCs, such as Na_xZ and K_xZ. Moreover, $Li_{4.4}Si$ and $Li_{4.4}Ge$ NCs were conformally encapsulated in carbon fibers; our future work is to test the promise of using these materials to mitigate the volume-fluctuation-induced poor cyclability problem confronted by Z anodes in lithium ion batteries.

Experimental Section

Materials: Lithium metal (Li, granular 4–10 mesh, 99%), silicon (Si, 325 mesh, 99%), hexane (anhydrous, 95%), *N*,*N*-dimethylformamide (DMF, anhydrous, 99.8%), polyacrylonitrile (PAN, $M_w \approx 150$k), hexyllithium (HL, 2.3 M in hexane), and triethylsilane (TES, 99%) were purchased from Aldrich. Germanium (Ge, pieces, 99.999%) and tin (Sn, 1.0 mm diameter wires, 99.999%) were purchased from ESPI. All chemicals were used as received.

Methods: Colloidal $Li_{4.4}Si$, $Li_{3.75}Si$, $Li_{4.4}Ge$, and $Li_{4.4}Sn$ NCs were synthesized by using a two-step protocol to separate surface protection from crystal formation. First, bare Li_xZ crystals were produced by milling lithium metal and Z elements.[43,64] Second, hexyllithium was added to passivate the generated Li_xZ NCs under the assistance of additional milling. All syntheses of $Li_{4.4}Z$ (and not $Li_{3.75}Si$) required 10% of extra lithium beyond stoichiometry. Typically, the controlled amounts of Li and Z (for instance, 0.2200 g of Li and 0.1839 g of Si for making $Li_{4.4}Si$) were mixed in an argon-

 © 2014 Wiley-VCH Verlag GmbH & Co. KGaA, Weinheim

filled milling jar, together with 3 mL of hexane as the lubricant to prevent the Li from sticking to the jar and the balls. The jar was mounted on a high-energy ball mill (SPEX Sample Prep, Mixer/Mill 8000M) outside of the glove box (MBraun LABstar) to mill 100 minutes for all Li_xZ except for $Li_{4.4}Sn$ (300 minutes). Afterward, a hexane solution of 2.3 M HL was added at the molar ratio of 8.8:1 for HL:$Li_{4.4}Z$ (or 4.8:1 for HL:$Li_{3.75}Si$) and the system was milled for another 100 minutes. The obtained black solution was centrifuged at 14.6 krpm for 20 minutes to collect the precipitate, which was further purified to remove the excess HL by repeating the hexane dispersion and centrifugation 3–4 times. Finally, the obtained colloidal Li_xZ NCs were dispersed in hexane for characterization.

$Li_{4.4}Si$ and $Li_{4.4}Ge$ NC-loaded carbon fibers (CFs) were synthesized by the electronspinning technique. First, two stock solutions of $Li_{4.4}Si$ (or $Li_{4.4}Ge$) NCs in DMF and PAN in DMF were made. Then, they were mixed and stirred for 10 minutes to get a homogenous, viscous solution containing 1 wt% of $Li_{4.4}Si$ (or $Li_{4.4}Ge$) NCs and 12 wt% (or 14 wt%) of PAN. This solution was loaded into a luer lock syringe with a stainless steel needle (14 gauge, ID = 1.70 mm). A flow rate of 1.5 mL h^{-1} was applied using a syringe pump (New Era Pump Systems, Inc.) to provide a constant flow rate. A direct voltage of 20 kV was applied using a Gamma high-voltage research power supply (model ES40P-20W/DAM, Ormond Beach, FL) between the needle and the copper foil collector positioned 10 cm away. The charged solution was sprayed out of the syringe and turned into fibers on the copper foil, due to the evaporation of DMF during the flight.[76] The synthesized fibers were then heated under argon in a tube furnace for 30 minutes at 250 °C to stabilize PAN and for 60 minutes at 600 °C to carbonize PAN, producing Li_xZ@C fibers.

Sample analysis and characterization: X-ray diffraction (XRD) patterns were collected on a Philips X'Pert X-Ray diffractometer using Cu K_α radiation ($\lambda = 0.154054$ nm). The samples were prepared in an argon-filled glove box by drop-casting Li_xZ colloidal solutions onto glass substrates. To prevent detrimental reactions due to the inevitable air exposure during measurements, the dried samples were immediately wetted with a few drops of mineral oil in the glove box. The background contribution from mineral oil was featured with a broad peak centered at 17.2° with a width from 10 to 25° and corrected before analysis. Transmission electron microscopy (TEM) was performed on a Phillips CM200 microscope with a built-in energy-dispersive X-ray (EDX) spectrometer (Princeton Gamma-Tech Prism). TEM samples were prepared in an argon glove box, by dropping Li_xZ colloidal solutions onto 400-mesh carbon-coated copper grids (Electron Microscopy Sciences, CF400-Cu). Fourier transform infrared (FTIR) spectroscopy was taken on a Thermo Scientific Nicolet iS50 spectrometer using the attenuated total reflection (ATR) mode for powder samples at a spectral resolution of 2 cm^{-1}. Scanning electron microscopy (SEM) images were taken on a field emission scanning electron microscope (FESEM, JEOL JSM-7000F). The particle sizes and size distributions of the synthesized Li_xZ NCs in the TEM images were analyzed using ImageJ software (National Institute of Heath, version 1.45 s). The diameters of the NCs were calculated from the two-dimensional projections.

Received: August 8, 2014
Revised: October 14, 2014
Published online: November 3, 2014

Keywords: anode materials · colloids · group 14 elements · nanoparticles · prelithiation

[1] J. M. Tarascon, M. Armand, *Nature* **2001**, *414*, 359 – 367.
[2] B. Xu, D. N. Qian, Z. Y. Wang, Y. S. L. Meng, *Mater. Sci. Eng. R* **2012**, *73*, 51 – 65.
[3] M. S. Whittingham, *Proc. IEEE* **2012**, *100*, 1518 – 1534.
[4] B. A. Boukamp, G. C. Lesh, R. A. Huggins, *J. Electrochem. Soc.* **1981**, *128*, 725 – 729.
[5] R. Yazami, P. Touzain, *J. Power Sources* **1983**, *9*, 365 – 371.
[6] L. Baggetto, P. H. L. Notten, *J. Electrochem. Soc.* **2009**, *156*, A169 – A175.
[7] J. Graetz, C. C. Ahn, R. Yazami, B. Fultz, *Electrochem. Solid-State Lett.* **2003**, *6*, A194 – A197.
[8] X. H. Liu, Y. Liu, A. Kushima, S. L. Zhang, T. Zhu, J. Li, J. Y. Huang, *Adv. Energy Mater.* **2012**, *2*, 722 – 741.
[9] B. Wang, B. Luo, X. Li, L. Zhi, *Mater. Today* **2012**, *15*, 544 – 552.
[10] I. A. Courtney, J. R. Dahn, *J. Electrochem. Soc.* **1997**, *144*, 2045 – 2052.
[11] W. M. Zhang, J. S. Hu, Y. G. Guo, S. F. Zheng, L. S. Zhong, W. G. Song, L. J. Wan, *Adv. Mater.* **2008**, *20*, 1160 – 1165.
[12] Y. H. Xu, Y. J. Zhu, Y. H. Liu, C. S. Wang, *Adv. Energy Mater.* **2013**, *3*, 128 – 133.
[13] N. C. Li, C. R. Martin, *J. Electrochem. Soc.* **2001**, *148*, A164 – A170.
[14] X. L. Wang, M. Feygenson, M. C. Aronson, W. Q. Han, *J. Phys. Chem. C* **2010**, *114*, 14697 – 14703.
[15] Y. Wang, J. Y. Lee, B. H. Chen, *J. Electrochem. Soc.* **2004**, *151*, A563 – A570.
[16] X. H. Liu, J. Y. Huang, *Energy Environ. Sci.* **2011**, *4*, 3844 – 3860.
[17] T. D. Hatchard, J. R. Dahn, *J. Electrochem. Soc.* **2004**, *151*, A838 – A842.
[18] C. K. Chan, X. F. Zhang, Y. Cui, *Nano Lett.* **2008**, *8*, 307 – 309.
[19] H. Wu, G. Yu, L. Pan, N. Liu, M. T. McDowell, Z. Bao, Y. Cui, *Nat. Commun.* **2013**, *4*, 1943.
[20] N. Liu, H. Wu, M. T. McDowell, Y. Yao, C. M. Wang, Y. Cui, *Nano Lett.* **2012**, *12*, 3315 – 3321.
[21] H. Wu, G. Chan, J. W. Choi, I. Ryu, Y. Yao, M. T. McDowell, S. W. Lee, A. Jackson, Y. Yang, L. B. Hu, Y. Cui, *Nat. Nanotechnol.* **2012**, *7*, 309 – 314.
[22] M. Yoshio, H. Y. Wang, K. Fukuda, T. Umeno, N. Dimov, Z. Ogumi, *J. Electrochem. Soc.* **2002**, *149*, A1598 – A1603.
[23] J. Xiao, W. Xu, D. Wang, D. Choi, W. Wang, X. Li, G. L. Graff, J. Liu, J.-G. Zhang, *J. Electrochem. Soc.* **2010**, *157*, A1047 – A1051.
[24] K. H. Seng, M. H. Park, Z. P. Guo, H. K. Liu, J. Cho, *Angew. Chem. Int. Ed.* **2012**, *51*, 5657 – 5661; *Angew. Chem.* **2012**, *124*, 5755 – 5759.
[25] C. K. Chan, X. F. Zhang, Y. Cui, *Nano Lett.* **2008**, *8*, 307 – 309.
[26] J. W. Wang, Y. He, F. F. Fan, X. H. Liu, S. M. Xia, Y. Liu, C. T. Harris, H. Li, J. Y. Huang, S. X. Mao, T. Zhu, *Nano Lett.* **2013**, *13*, 709 – 715.
[27] C. M. Wang, X. L. Li, Z. G. Wang, W. Xu, J. Liu, F. Gao, L. Kovarik, J. G. Zhang, J. Howe, D. J. Burton, Z. Y. Liu, X. C. Xiao, S. Thevuthasan, D. R. Baer, *Nano Lett.* **2012**, *12*, 1624 – 1632.
[28] X. H. Liu, L. Q. Zhang, L. Zhong, Y. Liu, H. Zheng, J. W. Wang, J. H. Cho, S. A. Dayeh, S. T. Picraux, J. P. Sullivan, S. X. Mao, Z. Z. Ye, J. Y. Huang, *Nano Lett.* **2011**, *11*, 2251 – 2258.
[29] C. K. Chan, H. L. Peng, G. Liu, K. McIlwrath, X. F. Zhang, R. A. Huggins, Y. Cui, *Nat. Nanotechnol.* **2008**, *3*, 31 – 35.
[30] U. Kasavajjula, C. S. Wang, A. J. Appleby, *J. Power Sources* **2007**, *163*, 1003 – 1039.
[31] J. H. Ryu, J. W. Kim, Y. E. Sung, S. M. Oh, *Electrochem. Solid-State Lett.* **2004**, *7*, A306 – A309.
[32] J. K. Lee, M. C. Kung, L. Trahey, M. N. Missaghi, H. H. Kung, *Chem. Mater.* **2009**, *21*, 6 – 8.
[33] Y. Hwa, W. S. Kim, S. H. Hong, H. J. Sohn, *Electrochim. Acta* **2012**, *71*, 201 – 205.
[34] L. F. Cui, R. Ruffo, C. K. Chan, H. L. Peng, Y. Cui, *Nano Lett.* **2009**, *9*, 491 – 495.
[35] J. C. Guo, X. L. Chen, C. S. Wang, *J. Mater. Chem.* **2010**, *20*, 5035 – 5040.

 © 2014 Wiley-VCH Verlag GmbH & Co. KGaA, Weinheim

[36] S. H. Ng, J. Z. Wang, D. Wexler, K. Konstantinov, Z. P. Guo, H. K. Liu, *Angew. Chem. Int. Ed.* **2006**, *45*, 6896 – 6899; *Angew. Chem.* **2006**, *118*, 7050 – 7053.
[37] X. L. Li, P. Meduri, X. L. Chen, W. Qi, M. H. Engelhard, W. Xu, F. Ding, J. Xiao, W. Wang, C. M. Wang, J. G. Zhang, J. Liu, *J. Mater. Chem.* **2012**, *22*, 11014 – 11017.
[38] B. Hertzberg, A. Alexeev, G. Yushin, *J. Am. Chem. Soc.* **2010**, *132*, 8548 – 8549.
[39] J. Y. Luo, X. Zhao, J. S. Wu, H. D. Jang, H. H. Kung, J. X. Huang, *J. Phys. Chem. Lett.* **2012**, *3*, 1824 – 1829.
[40] Y. S. He, P. F. Gao, J. Chen, X. W. Yang, X. Z. Liao, J. Yang, Z. F. Ma, *RSC Adv.* **2011**, *1*, 958 – 960.
[41] M. Holzapfel, H. Buqa, L. J. Hardwick, M. Hahn, A. Wursig, W. Scheifele, P. Novak, R. Kotz, C. Veit, F. M. Petrat, *Electrochim. Acta* **2006**, *52*, 973 – 978.
[42] Z. D. Zeng, N. Liu, Q. S. Zeng, Y. Ding, S. X. Qu, Y. Cui, W. L. Mao, *J. Power Sources* **2013**, *242*, 732 – 735.
[43] B. Key, R. Bhattacharyya, M. Morcrette, V. Seznec, J. M. Tarascon, C. P. Grey, *J. Am. Chem. Soc.* **2009**, *131*, 9239 – 9249.
[44] F. Wang, L. J. Wu, B. Key, X. Q. Yang, C. P. Grey, Y. M. Zhu, J. Graetz, *Adv. Energy Mater.* **2013**, *3*, 1324 – 1331.
[45] M. T. McDowell, Y. Cui, *Adv. Energy Mater.* **2011**, *1*, 894 – 900.
[46] M. T. McDowell, S. W. Lee, J. T. Harris, B. A. Korgel, C. M. Wang, W. D. Nix, Y. Cui, *Nano Lett.* **2013**, *13*, 758 – 764.
[47] S. C. Jung, Y. K. Han, *Phys. Chem. Chem. Phys.* **2011**, *13*, 21282 – 21287.
[48] H. Wu, G. Y. Zheng, N. A. Liu, T. J. Carney, Y. Yang, Y. Cui, *Nano Lett.* **2012**, *12*, 904 – 909.
[49] Y. X. Yin, S. Xin, Y. G. Guo, L. J. Wan, *Angew. Chem. Int. Ed.* **2013**, *52*, 13186 – 13200; *Angew. Chem.* **2013**, *125*, 13426 – 13441.
[50] J. Hassoun, J. Kim, D. J. Lee, H. G. Jung, S. M. Lee, Y. K. Sun, B. Scrosati, *J. Power Sources* **2012**, *202*, 308 – 313.
[51] Y. Yan, Y. X. Yin, S. Xin, J. Su, Y. G. Guo, L. J. Wan, *Electrochim. Acta* **2013**, *91*, 58 – 61.
[52] N. Liu, L. Hu, M. T. McDowell, A. Jackson, Y. Cui, *ACS Nano* **2011**, *5*, 6487 – 6493.
[53] T. H. Hwang, Y. M. Lee, B. S. Kong, J. S. Seo, J. W. Choi, *Nano Lett.* **2012**, *12*, 802 – 807.
[54] C. He, S. Wu, N. Zhao, C. Shi, E. Liu, J. Li, *ACS Nano* **2013**, *7*, 4459 – 4469.
[55] X. H. Liu, J. W. Wang, S. Huang, F. F. Fan, X. Huang, Y. Liu, S. Krylyuk, J. Yoo, S. A. Dayeh, A. V. Davydov, S. X. Mao, S. T. Picraux, S. L. Zhang, J. Li, T. Zhu, J. Y. Huang, *Nat. Nanotechnol.* **2012**, *7*, 749 – 756.
[56] Y. A. Yang, H. M. Wu, K. R. Williams, Y. C. Cao, *Angew. Chem. Int. Ed.* **2005**, *44*, 6712 – 6715; *Angew. Chem.* **2005**, *117*, 6870 – 6873.
[57] R. Nesper, H. G. von Schnering, *J. Solid State Chem.* **1987**, *70*, 48 – 57.
[58] H. Okamoto, *J. Phase Equilib. Diffus.* **2009**, *30*, 118 – 119.
[59] J. Sangster, C. W. Bale, *J. Phase Equilib.* **1998**, *19*, 70 – 75.
[60] J. Sangster, A. D. Pelton, *J. Phase Equilib.* **1997**, *18*, 289 – 294.
[61] M. Zeilinger, I. M. Kurylyshyn, U. Haussermann, T. F. Fassler, *Chem. Mater.* **2013**, *25*, 4623 – 4632.
[62] M. Zeilinger, D. Benson, U. Haussermann, T. F. Fassler, *Chem. Mater.* **2013**, *25*, 1960 – 1967.
[63] S. Dupke, T. Langer, R. Pottgen, M. Winter, H. Eckert, *Solid State Nucl. Magn. Reson.* **2012**, *42*, 17 – 25.
[64] S. Dupke, T. Langer, R. Pottgen, M. Winter, S. Passerini, H. Eckert, *Phys. Chem. Chem. Phys.* **2012**, *14*, 6496 – 6508.
[65] R. J. Ma, Y. F. Liu, Y. P. He, M. X. Gao, H. G. Pan, *J. Phys. Chem. Lett.* **2012**, *3*, 3555 – 3558.
[66] R. Tamori, N. Machida, T. Shigematsu, *J. Jpn. Soc. Powder Powder Metall.* **2001**, *48*, 267 – 273.
[67] P. R. Griffiths, J. A. d. Haseth in *Chemical Analysis: A series of Monograph on Analytical Chemistry and Its Applications*, 2nd ed. (Ed.: J. D. Winefordner), Wiley, Hoboken, **2007**.
[68] H. J. Reich, *Chem. Rev.* **2013**, *113*, 7130 – 7178.
[69] Y. L. Wang, C. Rong, J. P. Liu, *Nanotechnology* **2007**, *18*, 465701.
[70] T. Tsuzuki, P. McCormick, *J. Mater. Sci.* **2004**, *39*, 5143 – 5146.
[71] J. Li, J. R. Dahn, *J. Electrochem. Soc.* **2007**, *154*, A156 – A161.
[72] Y. D. Wang, J. Dahn, *J. Electrochem. Soc.* **2006**, *153*, A2314 – A2318.
[73] Y. Hashimoto, N. Machida, T. Shigematsu, *Solid State Ionics* **2004**, *175*, 177 – 180.
[74] J. E. Cloud, L. W. Taylor, Y. Yang, *RSC Adv.* **2014**, *4*, 24551 – 24559.
[75] D. M. Piper, T. A. Yersak, S. B. Son, S. C. Kim, C. S. Kang, K. H. Oh, C. M. Ban, A. C. Dillon, S. H. Lee, *Adv. Energy Mater.* **2013**, *3*, 697 – 702.
[76] X. W. Zhang, L. W. Ji, O. Toprakci, Y. Z. Liang, M. Alcoutlabi, *Polym. Rev.* **2011**, *51*, 239 – 264.
[77] J. Guo, Z. Yang, Y. Yu, H. D. Abuña, L. A. Archer, *J. Am. Chem. Soc.* **2013**, *135*, 763 – 767.
[78] S. Lee, J. Kim, B.-C. Ku, J. Kim, H.-I. Joh, *Adv. Chem. Eng. Sci.* **2012**, *2*, 275 – 282.

 © 2014 Wiley-VCH Verlag GmbH & Co. KGaA, Weinheim